International Journal of Control, Automation and Systems 16(1) (2018) 39-54
http://dx.doi.org/10.1007/s12555-016-0740-0
ISSN:1598-6446 eISSN:2005-4092
http://www.springer.com/12555

Dynamic Modeling and Inverse Optimal PID with Feed-forward Control in $\mathcal{H}_\infty$ Framework for a Novel 3D Pantograph Manipulator

Manar Lashin*, Mohamed Fanni, Abdelfatah M. Mohamed, and Tomoyuki Miyashita

Abstract: This paper affords dynamic modeling and control for a new 3D pantograph manipulator. The new manipulator possesses pure decoupled translational motions and it is characterized by large workspace to size ratio, high speed, rigidity, and accuracy. Euler-Lagrange first type method is used to get the dynamic model. However, the resulted dynamic model is too complex to be used in model-based control techniques. Therefore, a simplified nominal plant is proposed. It allows the inverse dynamic solution efficiently. However, an explicit form of the nominal Coriolis and centrifugal matrix cannot be obtained due to the complicated kinematic terms. Considering these dynamic characteristics as well as the required robust trajectory tracking performance of the manipulator, a new controller is proposed. The new controller is called inverse optimal PID with Feed-Forward Control which is designed in $\mathcal{H}_\infty$ framework. The new controller has the following merits; robustness, optimality, simple implementation, and efficient execution without the need of explicit forms of dynamic matrices. The extended disturbance in the proposed controller is smaller than that in the inverse optimal PID control (IPID) and contains one type of error contrary to the nonlinear robust motion controller (NRIC). The performance of the proposed controller is compared with those of IPID and NRIC controllers for different trajectories and payloads. The dynamic simulation results via co-simulation of MSC-ADAMS® and MATLAB®/Simulink software prove the robustness of the proposed controller against speed/payload variations. The proposed controller is found to have higher performance compared with IPID and NRIC controllers. These results assure the feasibility of the 3D pantograph manipulator with the proposed controller for pure translational tracking applications.

Keywords: Decoupled motions, $\mathcal{H}_\infty$ framework, inverse PID, NRIC, pantograph, parallel robot, robust control, robust controller, translational manipulator.

1. INTRODUCTION

In recent decades parallel manipulators have received great progress in their development due to their advantages over serial manipulator such as higher stiffness, higher accuracy, and lower inertia. Despite its advantages, parallel manipulators suffer from several major drawbacks such as small workspace, complex forward kinematics, complicated structures, and a high manufacturing cost [1]. Some applications such as pick-and-place requires the positioning of the robot end-effector without changing its orientation. Several studies have considered the design and synthesis of manipulators to meet this need such as Delta and Tsai manipulators [2, 3]. However, a major problem with these manipulators is the limited workspace relative to their volume. Moreover, the reduction of the DOFs can result in coupled motions of the movable platform which increase the complexity of the kinematic and dynamic analysis as well as the control technique [4]. Achieving the translational decoupling between actuators themselves is considered point of research interest. Gosselin and Kong [5] present a 3D translational parallel robot, with fully-decoupled input-output relations. Afterward, a series of decoupled 3D translational parallel mechanisms has been published [6–10]. A search of the literature revealed many manipulators that have the same functionality but with different structures such as Tripteron [9,11–13] and Pantopteron [14]. In [15], a novel 3D translational pantograph manipulator has been proposed. This innovative design combines, to some extent, the advantages of both serial and parallel manipulators. In addition, it has decoupled 3D translational mo-

Manuscript received November 28, 2016; revised March 8, 2017 and April 18, 2017; accepted May 6, 2017. Recommended by Associate Editor Yingmin Jia under the direction of Editor Yingmin Jia. The first author is supported by a scholarship from the Mission Department, Ministry of Higher Education of the Government of Egypt which is gratefully acknowledged.

Manar Lashin, Mohamed Fanni, and Abdelfatah M. Mohamed are with the Department of Mechatronics and Robotics Engineering, Egypt-Japan University of Science and Technology, E-JUST- Alexandria, Egypt (e-mails: {manar.lashin, mohamed.fanni, abdelfatah.mohamed}@ejust.edu.eg). Mohamed Fanni is on leave: Department of Production Engineering and Mechanical Design, Faculty of Engineering, Mansoura University, Mansoura, Egypt. Abdelfatah M. Mohamed is on leave: Department of Electrical Engineering, Faculty of Engineering, Assiut University, Egypt. Tomoyuki Miyashita is with Department of Modern Mechanical Engineering, Waseda University, Tokyo, Japan (e-mail: tomo.miyashita@waseda.jp).
* Corresponding author.

tions. This proposed manipulator has several useful characteristics over its competitive counterparts such as Delta and Tsai manipulators. It has higher workspace to size ratio comparable to that of a serial manipulator as well as linear decoupled inputs-outputs relationships. Dynamic modeling of this new manipulator is required to use an efficient control strategy to realize its benefits. The complexity of the dynamic model of most parallel manipulators prevents the use of model-based controllers. Furthermore, the proposed manipulator has a non-conventional structure with interconnected chains. This increases the complexity of the dynamic formulation which has not been investigated in the literature. The model-free controller did not provide a satisfying performance. In [16], PD type of fuzzy controller is applied for the proposed manipulator. However, the controller was not robust enough for high-speed applications and high payloads. The main challenge faced by many model-based controllers is the need of explicit forms of the dynamic model matrices. This is not easy to have, in particular, the Coriolis and centrifugal matrix, C-matrix, specially for parallel and interconnected manipulators as the proposed manipulator. Park and Chang [17] introduced $\mathcal{H}_\infty$ control of a Modified Computed Torque Control (MCTC) for Lagrangian systems and applied it on serial manipulator. However, this controller needs explicit forms of all dynamic matrices. Choi *et al* [18] highlights the need to bring the optimal control to industrial robots through PID controller particularly for trajectory tracking problem. He used the nonlinear $\mathcal{H}_\infty$ framework of Park and Chan [17] to prove the optimality and robustness of the PID controller for Lagrangian systems. He proposed a controller called inverse optimal PID (IPID) and applied it also for a serial manipulator. Contrary to [17], IPID does not need any dynamic matrices. In the same framework, Kim *et al* [19] proposed a new controller structure for robotics applications called Nonlinear Robust Internal Loop Controller (NRIC). He applied it successfully for a serial manipulator. NRIC does not need C-matrix but needs an explicit form of the inertia matrix, M-matrix. Thus, IPID and NRIC controllers suit the dynamic characteristics of the proposed manipulator and can be applied for its trajectory tracking control. However, the applications of both controllers on the proposed manipulator, as will be shown in this work, indicates a lake of accuracy and robustness, particularly in high speed applications. To solve this problem a new controller is proposed based on the same framework of the IPID controller called Feed-Forward Controller with Inverse Optimal PID (FFOPID) that consists of a Feed-Forward controller and IPID controller. For this controller, there is no need to have an explicit form of any dynamic matrices. The extended disturbance that used in the formulation of the trajectory tracking problem is smaller than that of IPID and is function of one error contrary to that of NRIC which is function of two types of errors. The performance of the proposed controller, FFOPID, is compared with those of IPID and NRIC controllers based on payload variations under different trajectories. For the dynamic simulation using MSC-ADAMS, three batches of trajectories are used. First trajectory is a quintic polynomial, second trajectory is composed of three sinusoidal signals of different frequencies (2-20 rad/sec), and the third one is the standard pick-and-place cycle of 25×305 mm in 0.5 sec. The new controller shows a higher tractability under high speed applications compared with IPID and NRIC. This paper is organized as follows: The description of the 3D translational pantograph manipulator is presented in Section 2. The kinematic analysis is discussed in Section 3. Dynamic formulation based on generalized Euler-Lagrange formulation is presented in Section 4 and the derivation of the nominal plant is discussed in Section 5. The control strategy is explained in Section 6, while the simulation results and discussion are presented and analyzed in Section 7. Finally, some concluding remarks and future research directions are given in Section 8.

2. DESCRIPTION OF THE 3D TRANSNATIONAL PANTOGRAPH MANIPULATOR

The proposed 3D translational pantograph manipulator is shown in Fig. 1 comprises of a pantograph mechanism with two types of parallelograms. One type of the parallelograms is acting on the pantograph plane. It is responsible for fixing the orientation of the end-effector in the plane of the pantograph. The other type of the parallelograms is acting on planes perpendicular to the pantograph plane and is responsible for fixing the orientation of the end-effector in a plane perpendicular to that of the pantograph. So, the end-effector has fixed orientation in 3D space. The pantograph mechanism with two parallelograms of the first type are shown in Fig. 1 by dark lines. All revolute joints in this linkage have horizontal axes. Four parallelograms of the second type are shown in Fig. 1 by gray lines. Two parallelograms are on each side of the pantograph mechanism to achieve symmetrical design and hence increases the torsional stiffness of the system. All main revolute joints of these second type parallelograms have vertical axes. The revolute joints with horizontals axes exist within these parallelograms are to facilitate the working of the original pantograph mechanism and the parallelograms of the first type. The extreme left horizontal link at end A is fixed to a horizontal slider acting along z-axis relative to another vertical slider acting along y-axis relative to the ground. The joint with vertical axis at B is attached to a horizontal slider acting along the x-axis. The extreme right horizontal link at end E is the end-effector that moves pure translational motions without changing the orientation according to the independent motions of the linear actuators acting on the three sliders. Figure 2 shows the CAD model of the proposed ma-

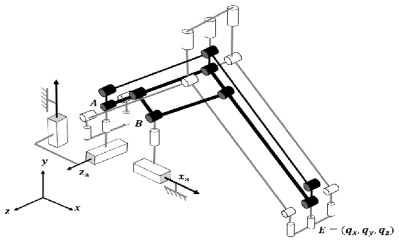

Fig. 1. Schematic diagram of the proposed pantograph.

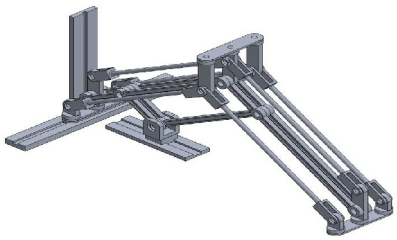

Fig. 2. 3D translational pantograph CAD model.

nipulator. On one side, the shape of the manipulator resembles that of a serial manipulator and enables having a large workspace. On the other side, all actuators are located on/near the base like a parallel manipulator which enables having low inertia links and consequently high speed, stiffness, and accuracy.

3. KINEMATIC ANALYSIS

In order to analyze the kinematics of the 3D translational pantograph manipulator, a fixed global reference system o-xyz is assigned as shown in Fig. 3. The following generalized coordinates $E = (q_x\ q_y\ q_z)$ denote the position of the end-effector. The purpose of the forward kinematics is to find the position of the moving platform q_x, q_y, q_z as a function of the actuated variables x_a, y_a, z_a. In parallel manipulator, the forward kinematics is complex due to the existence of the closed chains. In many parallel robots, this complexity does not yield closed form solutions. The proposed manipulator has simple forward/inverse kinematics relationships. The mechanical system in Fig. 3 has three input variables; $x_a = OB$, $y_a = A'A$, and $z_a = OA'$. The following two vector-loop closure equations can be written

$$\vec{OE} = \vec{OA} + \vec{AD} + \vec{DE}, \tag{1}$$

$$\vec{OE} = \vec{OB} + \vec{BF} + \vec{FE}, \tag{2}$$

where O is the origin of the fixed coordinate system O-xyz. The axes x, y, and z are parallel to the actuation axes of the three translational actuators. The position vector of the end-effector and the vector of the linear actuated joint variables are $E = [q_x, q_y, q_z]^T$ and $p = [x_a, y_a, z_a]^T$ respectively. Since the end-effector of the proposed manipulator

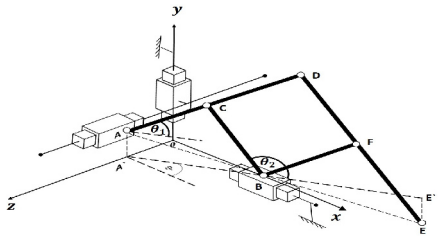

Fig. 3. Geometry of the 3D translational pantograph.

has translational motions only the rotation matrix becomes identity. Let $\overline{AC} = \overline{BC} = \overline{DF} = a$ and $\overline{CD} = \overline{BF} = \overline{FE} = b$ as design constraints. Loop equation (1) is used to obtain the following three scalar equations

$$q_x = (\cos\theta_1 - \cos\theta_2)(a+b)\cos\phi, \tag{3}$$

$$q_y - y_a = (\sin\theta_1 - \sin\theta_2)(a+b), \tag{4}$$

$$q_z - z_a = -(\cos\theta_1 - \cos\theta_2)(a+b)\sin\phi. \tag{5}$$

Similarly, three scalar equations can be derived from loop equation (2)

$$q_x - x_a = (\cos\theta_1 - \cos\theta_2)b\cos\phi, \tag{6}$$

$$q_y = (\sin\theta_1 - \sin\theta_2)b, \tag{7}$$

$$q_z = -(\cos\theta_1 - \cos\theta_2)b\sin\phi. \tag{8}$$

Dividing (3) by (6) to get the relation between the input actuator displacement x_a and the output displacement q_x along x-axis

$$q_x = M_x x_a, \tag{9}$$

where $M_x = 1 + \frac{b}{a}$ is the magnification factor of the input variable x_a. Similarly, from (4) and (7) and from (5) and (8), one gets the relationships between y_a and q_y and between z_a and q_z respectively.

$$q_y = M_y y_a,\ q_z = M_z z_a, \tag{10}$$

where $M_y = M_z = \frac{-b}{a}$ are the magnification factors of the input variables y_a and z_a respectively. The relations (9) and (10) illustrate the linearity between the input and output displacements as well as the decoupling of the translational motions. The angels ϕ, θ_1 and θ_2 are calculated according to the following equations:

$$\phi = atan2(z_a, x_a) \tag{11}$$

while

$$\theta_{1,2} = 2\,\mathrm{atan2}\left(\mp 2ay_a \pm \sqrt{4a^2y_a^2 - \left(\frac{x_a^2}{\cos\phi^2} + y_a^2\right)^2 + \frac{4a^2x_a^2}{\cos\phi^2}},\ \frac{x_a^2}{\cos\phi^2} + y_a^2 \pm \frac{2ax_a}{\cos\phi}\right). \tag{12}$$

4. DYNAMIC MODELING

There are different approaches that are commonly used in robotics to establish the dynamic model. Euler-Lagrange formulation, Newton-Euler formulation and the principle of virtual work. The Euler-Lagrange method of the first type probably is a better choice for the proposed manipulator. The proposed 3D pantograph manipulator is a special type of manipulators since it has interconnected structure rather than serial or parallel structures which increases its complexity. In Euler-Lagrange method of the first type, the equations are written in terms of a set of independent and redundant coordinates. Consequently, the method requires a set of constraint equations that relates the redundant coordinates to the independent coordinates. The constraint equations can be inspired from the kinematics of the proposed manipulator. The generalized coordinates vector, $\dot{q}$, is defined as $[\theta_1, \theta_2, \phi, x_a, y_a, z_a]^T$. The angles: θ_1, θ_2, and ϕ are the redundant coordinates while x_a, y_a and z_a are the independent joint variables. The constraint equations inferred from Fig. 3 are:

$$\Gamma_1 = (\frac{a+b}{a} - 1)\, x_a - b\cos\phi(\cos\theta_1 - \cos\theta_2), \quad (13)$$

$$\Gamma_2 = -(\frac{b}{a} + 1)\, y_a - (a+b)(\sin\theta_1 - \sin\theta_2), \quad (14)$$

$$\Gamma_3 = -(\frac{b}{a} + 1)\, z_a + (a+b)(\cos\theta_1 - \cos\theta_2)\sin\phi. \quad (15)$$

These constraint equations and their derivatives are adjoined to the main equations of motion using Lagrange multipliers λ_i. The equations of Euler-Lagrange of the first type are written as:

$$\frac{d}{dt}(\frac{\partial L}{\partial \dot{q}_j}) - \frac{\partial L}{\partial q_j} = \grave{Q}_j + \sum_{i=1}^{3} \lambda_i \frac{\partial \Gamma_i}{\partial q_j} \text{ for, } j = 1 \text{ to } 6, \quad (16)$$

where L is the Lagrangian which is expressed as the difference between the total kinetic energies K of links and the total potential energies U:

$$L = K - U.$$

$\grave{Q}_j$ is the generalized force associated with the generalized coordinate $\dot{q}_j$. Since there are no external forces associated with the redundant coordinates, the generalized force vector can be written as $\grave{Q} = [0\ 0\ 0\ f_x\ f_y\ f_z]^T$ where f_x, f_y, and f_z are the input forces acting on x-, y-, and z-slider respectively. For the inverse dynamics which are needed to implement the controllers considered in this work, Lagrangian multipliers, λ_i, are calculated from the first three equations in (16) as:

$$\sum_{i=1}^{3} \lambda_i \frac{\partial \Gamma_i}{\partial q_j} = \frac{d}{dt}(\frac{\partial L}{\partial \dot{q}_j}) - \frac{\partial L}{\partial q_j} \quad j = 1 \text{ to } 3. \quad (17)$$

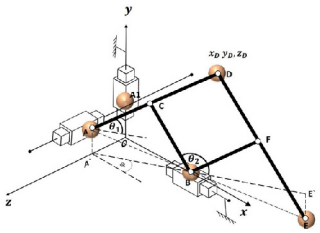

Fig. 4. Nominal plant for 3D pantograph manipulator.

Then, the actuator forces f_x, f_y and f_z are calculated from the last three equations in (16) as:

$$f_x = \frac{d}{dt}(\frac{\partial L}{\partial \dot{x}_a}) - \frac{\partial L}{\partial x_a} - \sum_{i=1}^{3} \lambda_i \frac{\partial \Gamma_i}{\partial x_a}, \ for\ j = 4\ to\ 6, \quad (18)$$

$$f_y = \frac{d}{dt}(\frac{\partial L}{\partial \dot{y}_a}) - \frac{\partial L}{\partial y_a} - \sum_{i=1}^{3} \lambda_i \frac{\partial \Gamma_i}{\partial y_a}, \ for\ j = 4\ to\ 6, \quad (19)$$

$$f_z = \frac{d}{dt}(\frac{\partial L}{\partial \dot{z}_a}) - \frac{\partial L}{\partial z_a} - \sum_{i=1}^{3} \lambda_i \frac{\partial \Gamma_i}{\partial z_a}, \ for\ j = 4\ to\ 6. \quad (20)$$

The closed-form dynamic equations of motion of the whole manipulator are expressed as:

$$M(q)\ddot{q} + C(q,\dot{q})\dot{q} + g(q) = Q, \quad (21)$$

where $M(q)$ is the 3×3 inertia matrix, $C(q,\dot{q})$ is the 3×3 Coriolis and centrifugal matrix and $g(q)$ is the gravity vector. In (21), Q and q are vectors $\in \mathbb{R}^3$, consist of the last three elements in $\grave{Q}$ and $\dot{q}$ respectively. The resultant equations, show that the actuator forces in x- and y-direction produce coupled motions in x- and y- direction while the actuator force in z-direction produces independent motion in z-direction. These results make the control task more difficult. The controller should recover these dynamic coupling between x- and y- directions. The dynamic model of the proposed 3D pantograph has a complicated kinematic terms. The symbolic expression of the Lagrangian or one of its derivatives has more than 25,000 character on MATLAB®. This makes the execution time of a single evaluation loop takes considerable long time which prevents the use of this dynamic model in practical control applications. To solve this problem a new method is proposed to get an accurate and simplified nominal plant.

5. NOMINAL PLANT DERIVATION

In this section, a method to obtain a simpler dynamic model for the proposed manipulator is explained. This nominal plant is established by assuming that the proposed 3D pantograph manipulator has five concentrated masses

at five points representing its inertia. The mass of each link is assumed to be concentrated equally at its two end-points like links AD and DE in Fig. 4 or concentrated at its midpoints like the sliders or the links perpendicular to the pantograph plane. In some cases, the concentrated masses are further replaced by other concentrated masses at different locations to decrease the total number of the concentrated masses. Take for example link BF in Fig. 4; first its mass is divided equally between two concentrated masses located at points B and F, then the concentrated mass at F is further divided into two masses located at points D and E according to the ratio of length FE to length FD. Figure 4 shows the five concentrated masses located at points A, A1, B, D, and E. Point A moves in y and z directions while points A1 and B moves in y- and x- directions respectively. Both points D and E moves in the three directions x, y, and z. The values of the concentrated masses are shown in Table 1. Afterward, the dynamic modeling using Euler-Lagrange of first type is applied using the generalized coordinates vector $[x_D, y_D, z_D, x_a, y_a, z_a]^T$, where

$$x_D = (a+b)\cos\theta_1\cos\phi, \tag{22a}$$
$$y_D = (a+b)\sin\theta_1 + y_a, \tag{22b}$$
$$z_D = -(a+b)\cos\theta_1\sin\phi + z_a. \tag{22c}$$

Using (11) and (12), one can get the constraints equations. The total kinetic energy of the concentrated masses is:

$$K = k_A + k_{A1} + k_B + k_D + k_E, \tag{23}$$

where

$$k_A = 0.5m_A(\dot{y}_a^2 + \dot{z}_a^2),\ k_{A1} = 0.5m_{A1}\dot{y}_a^2, \tag{24a}$$
$$k_B = 0.5m_B\dot{x}_a^2,\ k_D = 0.5m_D(\dot{x}_D^2 + \dot{y}_D^2 + \dot{z}_D^2), \tag{24b}$$
$$k_E = 0.5m_E((\frac{a+b}{a}\dot{x}_a)^2 + (\frac{-b}{a}\dot{y}_a)^2 + (\frac{-b}{a}\dot{z}_a)^2). \tag{24c}$$

The total potential energy of the manipulator is:

$$U = u_A + u_{A1} + u_B + u_D + u_E, \tag{25}$$

where

$$u_A = (m_A)\,g\,y_a,\ u_{A1} = (m_{A1})\,g\,y_a, \tag{26a}$$
$$u_B = 0,\ u_D = m_D\,g\,y_D,\ u_E = m_E\,g(\frac{-b}{a})\,y_a. \tag{26b}$$

The Lagrangian multipliers, λ_1, λ_2 and λ_3, are given by:

$$\lambda_1 = 5.263\ddot{x}_D,\ \lambda_2 = 5.263\ddot{y}_D + 51.63,\ \lambda_3 = 5.263\ddot{z}_D. \tag{27a}$$

The actuator forces f_x, f_y and f_z can be written as:

$$f_x = 96.9\ddot{x}_a + \lambda_1[\frac{c_1}{b_1} - \frac{c_1x_a^2}{b_2} + \frac{1.15x_ac_3 - a_7}{c_2}]$$
$$+ \lambda_3[\frac{c_1x_az_a}{b_2} - \frac{1.15z_ac_3 - a_7}{c_2}]$$
$$+ 1.15\lambda_2a_4b_7 - \frac{a_7}{b_3}, \tag{28}$$
$$f_y = 69.04\ddot{y}_a - \lambda_2[\frac{1.15c_{c5}a_8}{c7} - 1] - [1.15\lambda_1x_as_{c5}\frac{a_8}{c_6}]$$
$$+ [1.15\lambda_3z_as_{c5}\frac{a_8}{c_6}] + 96.03, \tag{29}$$
$$f_z = 67.81\ddot{z}_a - \lambda_3[\frac{0.575c_{c5}}{b_1} - a_9z_a^2 + \frac{1.15z_as_{c_5}e_3}{b_1c_7} - 1]$$
$$- \lambda_1[0.575x_az_aa_9 - \frac{1.15x_as_{c5}e_3}{b_1c_7}]$$
$$+ 1.15\lambda_2\frac{c_{c5}e_3}{c_7} \tag{30}$$

while a_i, b_i, c_i and e_i $i = 1, 2, ...etc$ are given in Appendix A.

The accuracy and efficiency of the simplified nominal plant are tested through dynamic simulation. The test is carried out using a trajectory composed of three sinusoidal motions with different frequencies for the three actuators acting in x-, y- and z-directions. This trajectory is applied for the dynamic models of both the proposed manipulator obtained by MSC-ADAMS® and the nominal plant. The two models are subjected to a trajectory with maximum frequency of 20 rad/sec as shown in Fig. 5. This test indicates that the nominal plant approximates the real model accurately even at high frequencies. According to this test, the nominal plant not only simplifies the complex dynamic model of the proposed manipulator but also alleviates the burden of the computation. Thus, the proposed simplified model can be implemented in practical

Table 1. The masses values at the five points of the nominal plant as illustrated by Fig. 4.

Lumped mass	[Kg]
m_A	2.6889
m_{A1}	1.232
m_B	1.4683
m_D	5.2628
m_E	2.886

Table 2. Comparison between the actuator forces calculated from MS-ADAMS®, Complete model and the Nominal Plant

Time	MS-ADAMS®,[N]	Complete model,[N]	Nominal Plant,[N]
Start	$f_x = -165.4$ $f_y = -198.41$ $f_z = -0.0331$	$f_x = -165.48$ $f_y = -198.27$ $f_z = -0.0372$	$f_x = -164.91$ $f_y = -198.95$ $f_z = -0.0329$
End	$f_x = -143.224$ $f_y = -177.457$ $f_z = -10.3705$	$f_x = -142.6$ $f_y = -177$ $f_z = -10.649$	$f_x = 142.791$ $f_y = -178.051$ $f_z = -10.339$

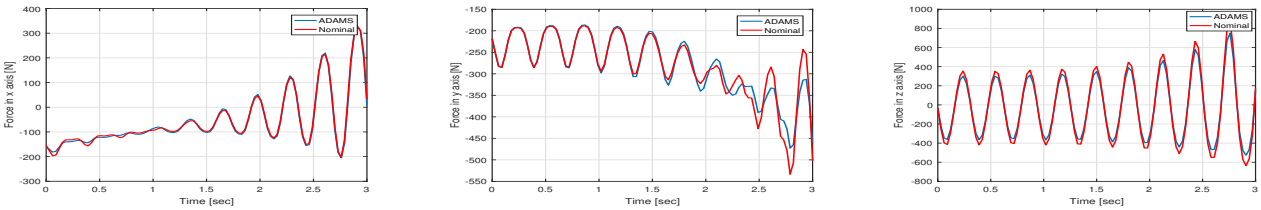

(a) Forces in x-axis (b) Forces in y-axis (c) Forces in z-axis

Fig. 5. Comparison between forces f_x, f_y and f_z of MSC-ADAMS® and those of the nominal plant for trajectory having maximum frequency of 20 rad/sec.

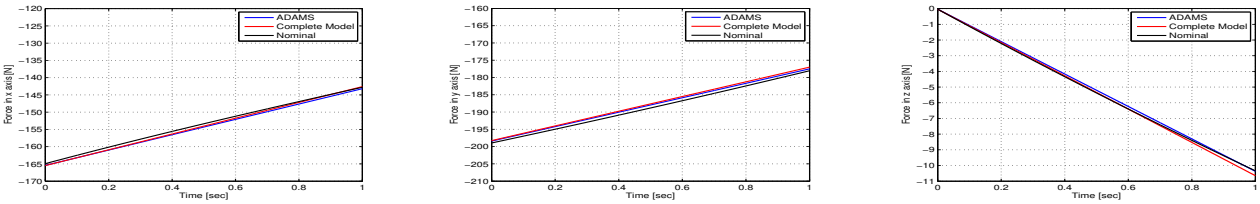

(a) Forces in x-axis (b) Forces in y-axis (c) Forces in z-axis

Fig. 6. Comparison between forces on the three orthogonal axes for MSC-ADAMS®, complete model and nominal plant.

applications to meet the demand of the real-time control. At the same time, the error between the responses of the real and simplified models as shown in Fig. 5 is within a reasonable range. This error will be recovered by the proposed controller as will be shown in Section.7. Another comparison between the complete dynamic model, nominal plant and the model obtained from MSC-ADAMS® are shown in Fig. 6. The results of the complete model that are generated using Euler-Lagrange of the first type represent the real dynamic model of the proposed manipulator accurately. Also, the simplified nominal plant approximates well the dynamics of the proposed manipulator. The values of these forces during the comparison are given in Table 2. As mentioned in the previous section, the complete dynamic model occupies large size in the workstation memory, more than 25,000 character for each symbolic expression such as $\dot{\theta}_1, \ddot{\theta}_1$...etc. The execution time of a single evaluation loop, using MATLAB/M-File®, for the actuator forces f_x, f_y and f_z takes about 90 min on a workstation with the following specs: Core i7, 16GB of RAM. This model consumes long execution time due to the use of symbolic toolbox in MATLAB/M-File® to calculate the time derivatives for the dynamic model variables, in addition to the long mathematical expressions of the angles θ_1 and θ_2. This results in a very big symbolic expression for the actuator forces f_x, f_y and f_z. This evaluation is done at least hundreds of times during each frequency test. One additional advantage of the proposed nominal plant lies in the ability to formulate the dynamic model using MATLAB/SIMULINK®. In this case, the mathematical equations can be built up easily in MATLAB/SIMULINK® and the time derivatives can be calculated using SIMULINK® engine more faster. Hence, the execution time reduces to be less than 0.04 msec. The calculation speed of the robot dynamics is essential for high-speed practical applications such as pick-and-place operation which requires a robust controller scheme to be applied. Consequently, the nominal plant makes it easy to apply model-based control on the proposed manipulator using MATLAB/SIMULINK® for high-speed applications.

6. INVERSE OPTIMAL PID WITH FEED-FORWARD CONTROLLER IN H_∞ FRAMEWORK

As shown in the previous section, the nominal plant approximates well the dynamics of the proposed manipulator. However, the symbolic extraction of its C-matrix (Coriolis and Centrifugal matrix) is not possible because of the complicated kinematics terms. Using Euler-Lagrange method of the first type enables the calculation of the inverse dynamics efficiently without the need of explicit dynamic matrices. So, for a search of a suitable controller for the proposed manipulator, such dynamic characteristics should be considered. As a first trial, the PID controller which is commonly used in industrial robots is investigated. Choi *et al* [18] used the nonlinear H_∞ framework to prove the optimality and robustness of the PID controller. Since they used inverse optimization method rather than direct optimization method, this controller is named inverse optimal PID (IPID) controller. They provide conditions for extended disturbance input-to-state stability (EISS). Unfortunately, the application of IPID for our proposed robot, as will be shown later

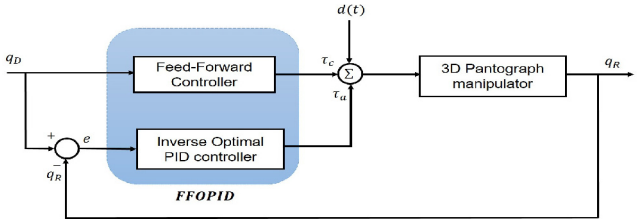

Fig. 7. Structure of the FFOPID.

indicates lake of robustness during high robot speed. In the same framework, Park and Chang [17] introduced H_∞ control of a Modified Computed Torque Control (MCTC). This controller consists of two parts.

The first part compensates the estimated torques while the second part is exactly the IPID controller. However, we could not apply this controller for the proposed manipulator, since it requires an explicit form of C-matrix of the nominal plant which is not available in our case. In the same framework, Kim *et al* [19] introduced Nonlinear Robust Internal Loop Compensator (NRIC). This controller consists of two parts. The first part is a Computed Torque Control (CTC) of a nominal plant, while the second part is exactly IPID controller. Since CTC requires the explicit form of the inertia matrix of the nominal plant only which is available in our case, we could apply this controller to the proposed manipulator. However, the results, as will be shown later in simulation section, are not encouraging. This can be attributed to many factors such as the two types of errors contained in the NRIC extended disturbances and the large number of gains to be tuned. It is to be noted that all the above-described controllers were not tested on parallel or interconnecting manipulators. They were tested solely on serial manipulators. The above mentioned unsuccessful results motivate us to develop a new controller in the same framework that is suitable for the proposed manipulator and its special dynamic characteristics. Fig. 7 shows the structure of the proposed controller. The controller consists of two parts: the first part is a Feed-Forward controller of the nominal plant while the second part is the IPID controller. On one hand, the Feed-Forward controller does not need an explicit form of any dynamic matrices when Euler-Lagrange method of the first type is used. This makes the calculation possible and faster. On the other hand, as shown later in the equations, the extended disturbance is smaller than the case of IPID and contains one type of error. This has positive consequences on the robustness of the controller. In this section, the design of the proposed controller is investigated and its optimality and stability are discussed. Let the closed loop dynamics of the proposed system be written as:

$$\tau_c + \tau_a = M_R(q_R)\ddot{q}_R + C_R(q_R,\dot{q}_R)\dot{q}_R + g_R(q_R) + d(t), \tag{31}$$

where M_R, C_R and g_R are the inertia matrix, Coriolis and centrifugal matrix and the gravitational vector respectively for the real plant and $d(t)$ is the external disturbance. The controller term τ_c is designed as a Feed-Forward control torque that is generated from the dynamic model of the nominal plant in which the desired configurations $q_D, \dot{q}_D, \ddot{q}_D$ are the required input:

$$\tau_c = M_N(q_D)\ddot{q}_D + C_N(q_D,\dot{q}_D)\dot{q}_D + g_N(q_D), \tag{32}$$

where M_N, C_N and g_N are the inertia matrix, Coriolis and centrifugal matrix and the gravitational vector respectively for the estimated nominal plant. It is to be noted that Euler-Lagrange method of the first type is used here to calculate τ_c where no explicit form of the above matrices are needed. By subtracting (32) from (31), the torque, τ_a, can be written as:

$$\tau_a = \widetilde{M}(\ddot{q}_R - \ddot{q}_D) + \widetilde{C}(\dot{q}_R - \dot{q}_D) + \widetilde{g} + d(t), \tag{33}$$

where $\widetilde{M} = M_R - M_N$, $\widetilde{C} = C_R - C_N$, $\widetilde{g} = g_R - g_N$. The extended disturbances including parameters uncertainties, nonlinearities and the external disturbances $d(t)$ are formulated here as:

$$\begin{aligned}\omega(t,\dot{e},e,\int e) =& \widetilde{M}\ddot{q}_D + M_R(K_P\dot{e} + K_I e) + \widetilde{C}\dot{q}_D \\ &+ C_R(K_P e + K_I\int e\,dt) + \widetilde{g} + d(t),\end{aligned} \tag{34}$$

where K_P, K_I are diagonal constant matrices and the tracking error is defined as $e = q_D - q_R$. The extended disturbance ω is assumed to be bounded and the configuration derivatives $\dot{q}_D, \dot{q}_R$ also are considered bounded. The resultant system dynamics becomes:

$$M_R(q_R)\dot{s} + C_R(q_R,\dot{q}_R)s = \omega + u, \tag{35}$$

where $u = -\tau_a$ and $s = \dot{e} + K_P e + K_I\int e dt$. If the state vector is defined as: $x = [x_1\ x_2\ x_3]^T = [\int e\ e\ \dot{e}]^T \in \mathbb{R}^{3n}$, the state-space representation of (35) can be found as:

$$\dot{x} = A(x,t)x + B(x,t)\omega + B(x,t)u, \tag{36}$$

where

$$A = \begin{bmatrix} 0 & I & 0 \\ 0 & 0 & I \\ -M^{-1}CK_I & -M^{-1}CK_P - KI & -M^{-1}C - K_P \end{bmatrix},$$

$$B = \begin{bmatrix} 0 \\ 0 \\ M^{-1} \end{bmatrix}.$$

Consider this general H_∞ performance index:

$$\int_0^\infty [x^T Q(x,t)x + u^T R(x,t)u]\,dt \le \gamma^2 \int_0^\infty \omega^T\omega\,dt, \tag{37}$$

where Q is a state weighting matrix, R is the control input weighting, and γ means L_2-gain. The Hamilton-Jacobi-Isaacs (HJI) equation for this performance index and Lyapunov function were suggested previously [20]:

$$HJI = V_t + V_x Ax + \frac{1}{2\gamma^2} V_x BB^T V_x^T - \frac{1}{2} V_x BR^{-1} B^T V_X^T + \frac{1}{2} x^T Qx = 0 \quad (38)$$

with a smooth function $V(x,t) > 0$, $V(0,t) = 0$, $V_t = \frac{\partial V}{\partial t}$ and $V_x = \frac{\partial V}{\partial x}$. $u = -R^{-1}B^T V_x^T$. This controller, u, minimizes the H_∞ performance index (37) and the Lyapunov function is $V(x,t) = x^T P(x,t)x$ where

$$P = \begin{bmatrix} K_I M_R K_I + K_I K_P K & K_I M_R K_P + K_I K & K_I M_R \\ K_P M_R K_I + K_I K & K_P M_R K_P + K_P K & K_P M_R \\ M_R K_I & M_R K_P & M_R \end{bmatrix}. \quad (39)$$

The following conditions should be satisfied:

1) $K, K_P, K_I > 0$, constant diagonal matrices,
2) $K_P^2 > 2K_I$.

This gives the differential Riccati equation:

$$\dot{P} + A^T P + PA - PBR^{-1}B^T P + Q = 0. \quad (40)$$

The weighting matrices Q and R will be inversely found from the differential Riccati equation. If the weighting matrix R is defined as:

$$R = (K + \frac{1}{\gamma^2} I)^{-1},$$

where I is the identity matrix, then the weighting matrix Q can be obtained from the differential Riccati equation inversely.

$$Q = \begin{bmatrix} K_I^2 KI & 0 & 0 \\ 0 & (K_P^2 - 2K_I)KI & 0 \\ 0 & 0 & KI \end{bmatrix}.$$

Choi *et al* [18] proved that if the IPID controller satisfying the following conditions:

1) $K, K_P, K_I > 0$, constant diagonal matrices,
2) $K_P^2 > 2K_I$,
3) $\gamma > 0$

is applied to the Lagrangian system (36), the closed-loop control system is EISS. Finally the proposed Feed-Forward control torque of (32), with the IPID can be expressed as:

$$\tau_c + \tau_a = M_N \ddot{q}_D + C_N \dot{q}_D + g_N + (K + \frac{1}{\gamma^2}) \left(\dot{e} + K_P e + K_I \int e \right), \quad (41)$$

The IPID that introduced by Choi *et al* [18] to solve trajectory tracking problem for complex mechanical systems has the following form:

$$u = -(K + \frac{1}{\gamma^2}) \left(\dot{e} + K_P e + K_I \int e \right). \quad (42)$$

The extended disturbances [18] can be written as:

$$\omega(t, \dot{e}, e, \int e) = M(q)(\ddot{q}_D + K_P \dot{e} + K_I e) + C(q, \dot{q}) \left(\dot{q}_D + K_P e + K_I \int e \right) + g(q) + d(t). \quad (43)$$

It is clear that the extended disturbance formulated in the proposed controller here (34) is smaller than that of IPID (43). Therefore, the performance of the proposed control is expected to be higher than that of IPID control as will be illustrated in the next section. For the NRIC controller proposed by Kim *et al* [19], the extended disturbance is expressed as:

$$\omega = M_R(M_N^{-1} - M_R^{-1} - K_P \dot{e}_R N - K_I e_{RN})\tau_c + C_R((C_R^{-1} M_R M_N^{-1} C_R - I)\dot{e}_{DN} - K_P e_{RN} - K_I \int e_{RN}) + (g_R - M_R M_N^{-1} g_N) + (C_R - M_R M_N^{-1} C_N)\dot{q}_D + d(t). \quad (44)$$

The notation R and N refers to real and nominal plants respectively. The overall control law for NRIC utilizing CTC as outer loop controller is:

$$u = \hat{M}_N(\ddot{q}_D + k_1 \dot{e}_{DN} + k_2 e_{DN}) + \hat{C}_N \dot{q}_N + \hat{g}_N + (K + \frac{1}{\gamma^2})(\dot{e}_{RN} + K_P e_{RN} + K_I \int e_{RN}). \quad (45)$$

As shown in (44), there are two types of errors, e_{DN} and e_{RN}. e_{DN} is the error between desired and nominal plant states, while e_{RN} is the error between real plant and nominal plant states. Also, as shown in (45) there are a large number of gains to be tuned compared to IPID and the proposed FFIPID controllers. In the next section, the three controllers IPID, NRIC (with CTC) and the proposed FFOPID controllers are applied to the proposed manipulators and their performances are compared. A realistic MSC-ADAMS ® model for the proposed manipulator is used as the real plant in the simulation studies.

7. SIMULATION STUDY AND DISCUSSION

The performance of the proposed controller, FFOPID, is tested and compared with NRIC and IPID controllers where three different trajectories are used. The first trajectory is a quintic polynomial of 0.5 sec duration while the second one is generated by three combined sinusoidal signals with different frequencies. The comparison is done for the first two trajectories at no payload condition and at a maximum payload of 4 kg. The third trajectory is a standard pick-and-place cycle of 25×305 mm in 0.5 sec. One of the most popular trajectories for industrial robots such as Delta robot is the pick-and-place

trajectory. So, the proposed controller will be tested for this trajectory. The total number of pick-and-place cycles that can be done by the robot per unit time in addition to the position error during this motion are important factors to judge the suitability for industrial applications. There are many industrial applications that can be achieved via typical pick-and-place motion such as; manipulating, inspecting, classifying, assembling, packing, and sorting the products [21]. The model of the proposed manipulator is built using SOLIDWORKS® and exported to MSC-ADAMS® to establish the nonlinear dynamic model accurately. Thereafter the co-simulation environment between MSC-ADAMS® and MATLAB® is set for building a virtual environment to validate different control schemes. The input variables are the actuators' forces which applied to the model in MSC-ADAMS®. They are calculated in MATLAB® based on the control architectures which are discussed in the previous section. The designing procedures of the new controller, FFOPID, include two parts: the Feed-Forward controller and the IPID controller. Choi *et al* [18] suggested some tuning rules and performance limitations for the IPID controller which will be taken into account to determine the gain matrices K, K_p and K_I. The system error vector, $[e_x, e_y, e_z]^T$, is inversely proportional to the magnitude of a state-weighting matrix, while the control effort is directly proportional to this magnitude. Therefore, there is a tradeoff between the system performance and control effort. The output of the controller is denoted by a three-dimensional wrench in the joint space $Q = [f_x\, f_y\, f_z]$. First, the proposed manipulator is tested for 'quintic' polynomial trajectory although the cubic-polynomial is commonly used in robotics context for trajectory tracking validation. However, its jerk is discontinuous and this may lead to vibration that deteriorates manipulator performance. Therefore, jerk continuity is desirable to improve control performance of manipulators. In [22], a fifth-order 'quintic' polynomial is proposed for a given path. The trajectory is given as:

$$\lambda(t) = a_1 t^5 + a_2 t^4 + a_3 t^3 + a_4 t^2 + a_5 t + a_6. \tag{46}$$

This results in a quadratic function of jerk, which is continuous and second-order differentiable

$$\dddot{\lambda} = 60 a_1 t^2 + 24 a_2 t + 6 a_3. \tag{47}$$

The tracking errors at the two payload conditions are shown in Figs. 8 and 9. As illustrated by these figures, the FFOPID controller has the best performance in-terms of the tracking error, followed by the IPID and lastly the NRIC. This difference in the performance of the three controllers becomes clearer when the payload is increased to the maximum value 4 kg. The control efforts are depicted in Figs. 10 and 11 at no payload and with maximum payload respectively. The FFOPID controller and IPID controller have smooth control forces in contrast to

Table 3. The maximum tracking error for NRIC, IPID and FFOPID at the end-effector during no payload and maximum payload, respectively.

Trajectory No.	NRIC, [m]	IPID, [m]	FFOPID, [m]
2 [rad/sec], No-payload	0.0049	0.0013	4.9×10^{-4}
2[rad/sec], Max. payload	0.0066	0.0021	6.6×10^{-4}
6[rad/sec], No-payload	0.0046	0.001	4.6×10^{-4}
6[rad/sec], Max. payload	0.0048	0.002	6.6×10^{-4}
20 [rad/sec], No-payload	0.0069	0.0016	8.1×10^{-4}
20 [rad/sec], Max. payload	0.0079	0.0033	0.002
Quintic, 0.5sec, No-payload	0.0039	0.0014	7.3×10^{-4}
Quintic, 0.5sec, Max. payload	0.0039	0.0023	8.3×10^{-4}

NRIC controller. Although FFOPID controller consumes higher actuator forces than IPID during quintic polynomial trajectory, they are still within the selected actuators ranges. Second, a combination of three sinusoidal signals with different frequencies is applied to the proposed manipulator in three stages. The frequency content of the trajectory is increased gradually from one stage to another up to 20 rad/sec for robustness validation under various frequencies. At the first stage, the maximum frequency of the trajectory is set to be 2 rad/sec under no payload and maximum payload as shown in Figs. 12(a) and 12(b). The errors are shown in Figs. 13 and 14 under the two payload conditions. According to these figures the maximum error is 0.0066 m, this occurs under maximum payload with NRIC controller, then the IPID controller gives 0.0021 m. The FFOPID controller gives a maximum error of 6.6×10^{-4} m at the maximum payload. The frequency of the first trajectory is small, nevertheless, the IPID controller and NRIC have a higher tracking error than FFOPID. Figures 15 and 16 show the control force of each actuator which is within the selected actuator range. At the second stage, the maximum frequency is increased to be 6 rad/sec. The errors in motions for the three actuators are shown in Figs. 17 and 18 during no payload and maximum payload respectively. These figures show that the FFOPID has the smallest error in all axes during the two cases of payloads while the NRIC shows the highest error in y-direction and the IPID has the highest error in z-direction. Figures 19 and 20 show the actuator forces in x-, y- and z-directions for the three controllers. The NRIC controller consumes the highest control forces for the three actuators which are changing rapidly. In the practical environment, the rapid change in actuator forces has undesired effects on the motors. Both the IPID and FFOPID controllers have smooth behavior besides FFOPID, in most cases, consumes lower actuators' forces. At the third stage, the tracking ability for NRIC and IPID start to vanish when the maximum fre-

quency becomes 20 rad/sec as shown in Fig. 21 while FFOPID shows high robustness and small tracking error during high frequency trajectories at no payload condition. Figure 22 shows the three controllers with maximum payload at frequency of 20 rad/sec. Although this frequency is high and the manipulator at the maximum payload case, the proposed controller can keep the best performance and outperforms the other controllers in-terms of tracking error and tracking performance. According to Figs. 23 and 24, the power consumption of the actuators particularly at z-direction at which the frequency becomes 20 rad/sec in increased rapidly. The NRIC controller has non-smooth performance in control force. The best tracking performance is for the proposed controller, FFOPID, and this is shown in Table 3 which illustrates the maximum tracking error for NRIC, IPID and FFOPID. IPID comes in second place followed by NRIC. The total weight of the proposed manipulator is 6.67 kg which is localized mainly at the base. Nevertheless, the proposed controller can recover the maximum payload which is 4 kg efficiently. Moreover, the FFOPID can recover the dynamic coupling between x- and y- directions thoroughly. Further improvements are currently a research target to get a balanced/light weight 3D pantograph that will be expected to perform better in-terms of tracking error and control effort. Afterward, the FFOPID controller is tested for standard pick-and-place cycle of 25×305 mm in 0.5 sec as shown in Fig. 25 where the maximum error is found to be 0.1 mm at the end-effector with a payload of 4 Kg. The new manipulator is designed to work at high speed applications, so the speed of the trajectory is considered during all trajectories. The dynamic simulation results show the ability of the proposed 3D pantograph manipulator to give a large workspace as serial robot and high speed and rigidity as parallel robot. Finally, the robustness of the proposed controller, FFOPID is tested against Gaussian noise applied on the measured position vector of the actuators $[x_a, y_a, z_a]$ with a variance of 10^{-9}. Figure 26 shows the joint space errors in each axis. These results indicate that the controller can recover the noise effect with small tracking errors. However, the control signal is increased to suppress noise effect. The proposed controller, FFOPID, shows a satisfactory performance during trajectory tracking and high-speed pick-and-place cycle. It compensates the difference between the nominal plant and the real dynamics model that imported from MSC-ADAMS®. The FFOPID controller is applicable not only for the proposed 3D pantograph but also for any complicated Lagrangian systems in which we can not use an explicit form of the dynamic model matrices.

8. CONCLUSIONS

In this paper, an inverse optimal PID controller design in $\mathcal{H}_\infty$ framework with a feed-forward controller is proposed for a novel 3D pantograph manipulator. The new manipulator integrates the merits of both serial and parallel manipulators. It posses pure decoupled translational motions and it is characterized by large workspace to size ratio as well as high speed, rigidity, and accuracy. The dynamic model for a novel 3D translational manipulator is presented based on Euler-Lagrange of first type method. Moreover, a straightforward method to get an approximated nominal plant for the dynamic model is presented to be used for model-based control methods. The designing procedures of the proposed controller, feed-forward control with inverse-optimal PID in $\mathcal{H}_\infty$ framework is presented with its stability analysis. This new controller combines many features such as straightforward implementation, robustness, optimality, and efficient execution without the need of explicit forms of dynamic matrices. The performance of the proposed controller is compared with those of nonlinear robust motion controller, NRIC, and inverse-optimal PID controller for different trajectories with different frequencies and payload variations. The comparison indicates that the proposed controller outperforms the other two controllers. The robustness of the proposed controller against speed/payload variations are verified through dynamic simulation using MSC-ADAMS® and MATLAB®.

Consequently, the feasibility of the whole system is assured for pure translational tracking applications. The future research goal is to complete the experimental setup and investigates the dynamics of the controller during the experimental work to validate the theoretical results. Study the possibility of actuator faults and its modeling methods particularly during the experimental validation [23–26] is a part of our future work. In the same sense, there is a need to implement a filtering stage for the proposed control scheme [27].

APPENDIX A: KINETIC AND POTENTIAL ENERGIES

The kinetic energy of i link can be computed according to the following equation:

$$k_i = \frac{1}{2} m_i (\dot{x}_i^2 + \dot{y}_i^2 + \dot{z}_i^2) + \frac{1}{2} \omega_{1,2} R_{1,2} I_i R_{1,2}^T \omega_{1,2}^T, \tag{A.1}$$

where $\dot{x}_i, \dot{y}_i, \dot{z}_i$ are the linear velocity of each link along x-, y- and z-directions respectively and I_i is the inertia matrix of link i. There are two rotation matrices R_1 and R_2:

$$R_1 = Rot_{y,\phi} Rot_{z,(\pi/2+\theta_1)} Rot_{x,(\pi/2)}, \tag{A.2}$$

$$R_2 = Rot_{y,\phi} Rot_{z,(\theta_2-\pi/2)} Rot_{x,(\pi/2)}, \tag{A.3}$$

and two angular velocities vectors ω_1 and ω_2 are calculated from the skew-symmetric matrix Ω_1 and Ω_2

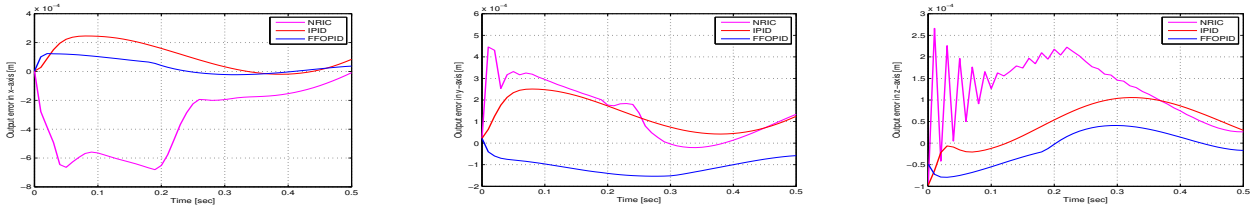

(a) Error in x-direction (b) Error in y-direction (c) Error in z-direction

Fig. 8. Joint space errors during quintic polynomial trajectory tracking control with no payload.

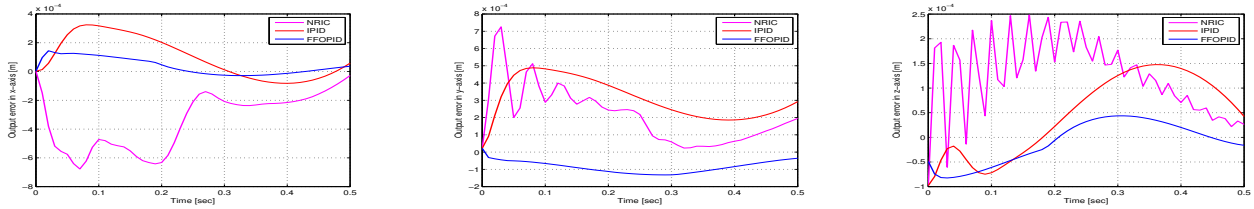

(a) Error in x-direction (b) Error in y-direction (c) Error in z-direction

Fig. 9. Joint space errors during quintic polynomial trajectory tracking control with maximum payload 4 kg.

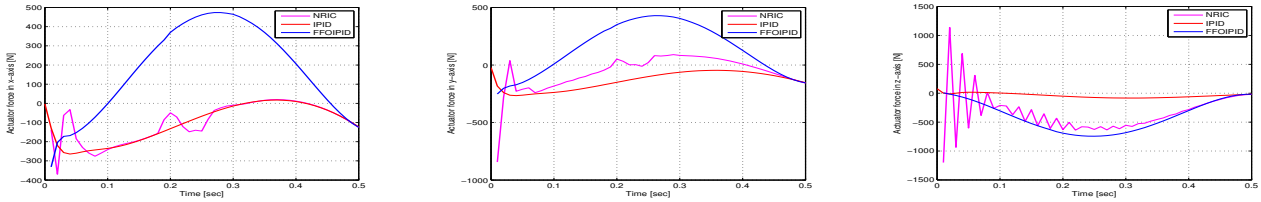

(a) Actuator force in x-direction (b) Actuator force in y-direction (c) Actuator force in z-direction

Fig. 10. Actuator forces for quintic polynomial trajectory tracking control with no payload.

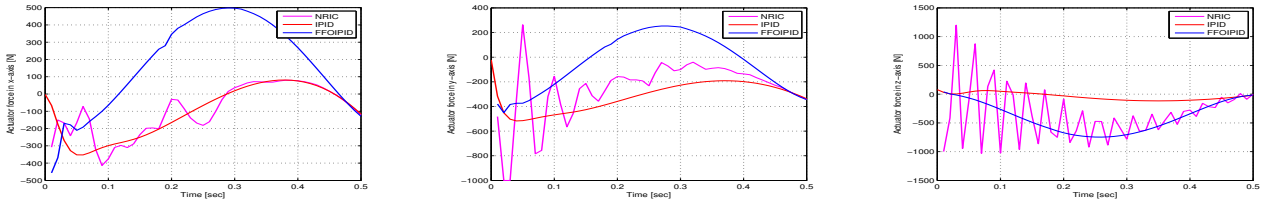

(a) Actuator force in x-direction (b) Actuator force in y-direction (c) Actuator force in z-direction

Fig. 11. Actuator forces for quintic polynomial trajectory tracking control with maximum payload 4 kg.

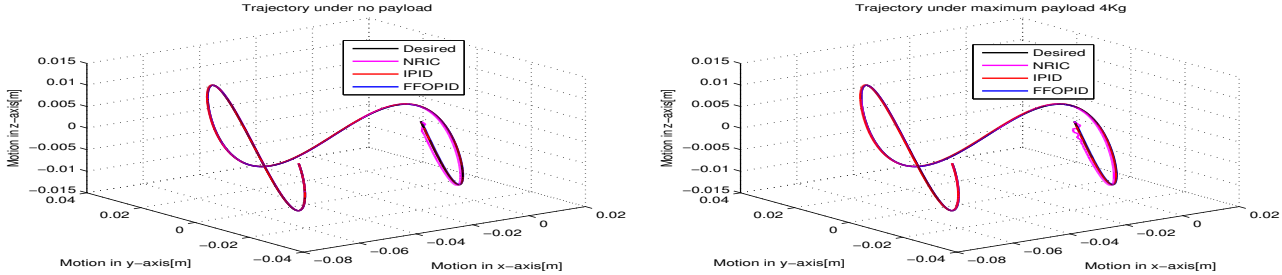

(a) No payload condition (b) Maximum payload condition

Fig. 12. Tracking control of trajectory with maximum frequency of 2 rad/sec.

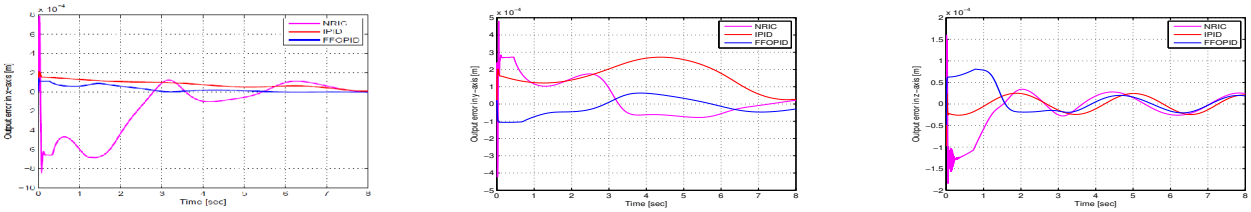

(a) Error in x-direction (b) Error in y-direction (c) Error in z-direction

Fig. 13. Joint space errors during trajectory tracking control with no payload and maximum frequency of 2 rad/sec.

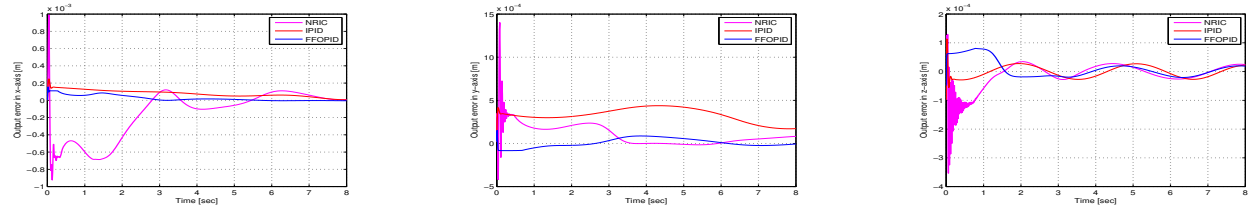

(a) Error in x-direction (b) Error in y-direction (c) Error in z-direction

Fig. 14. Joint space errors during trajectory tracking control with maximum payload and maximum frequency of 2 rad/sec.

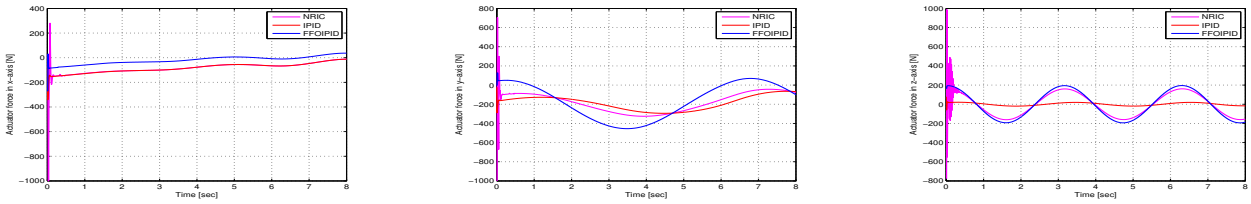

(a) Actuator force in x-axis (b) Actuator force in y-axis (c) Actuator force in z-axis

Fig. 15. Actuator forces for trajectory tracking control under no payload with maximum frequency of 2 rad/sec.

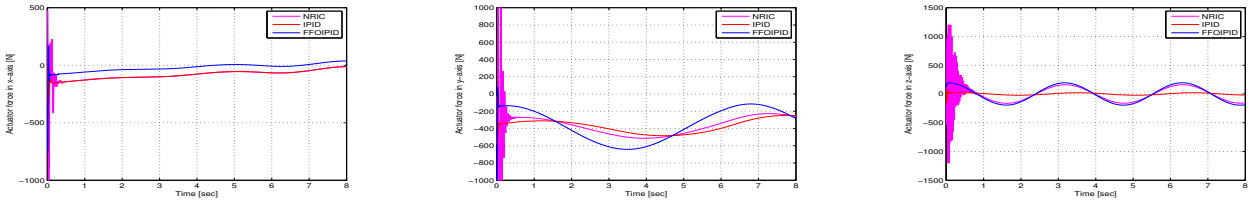

(a) Actuator force in x-axis (b) Actuator force in y-axis (c) Actuator force in z-axis

Fig. 16. Actuator forces for trajectory tracking control under maximum payload with maximum frequency of 2 rad/sec.

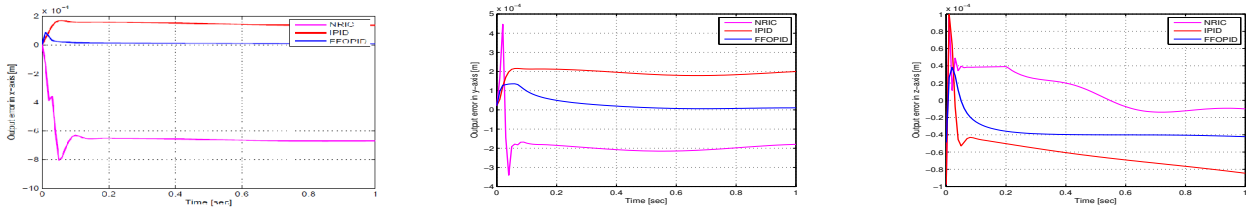

(a) Error in x-direction (b) Error in y-direction (c) Error in z-direction

Fig. 17. Joint space errors for NRIC, IPID and FFOPID during trajectory tracking control with no payload and maximum frequency of 6 rad/sec.

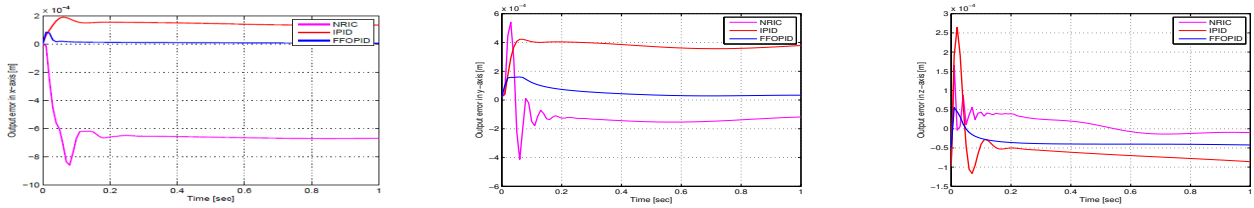

(a) Error in x-direction (b) Error in y-direction (c) Error in z-direction

Fig. 18. Joint space errors for NRIC, IPID and FFOPID during trajectory tracking control with maximum payload and maximum frequency of 6 rad/sec.

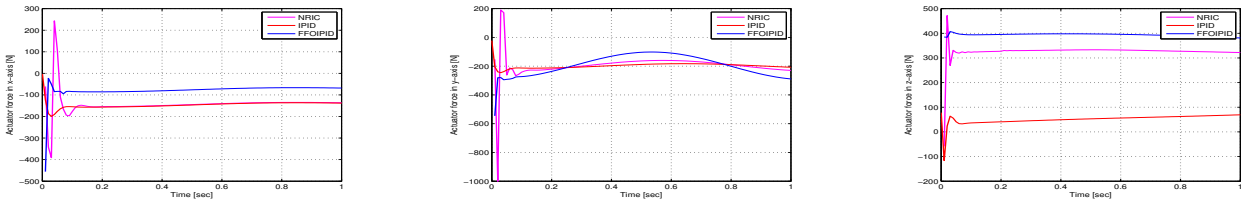

(a) Actuator force in x-axis (b) Actuator force in y-axis (c) Actuator force in z-axis

Fig. 19. Actuator forces for trajectory tracking control under no payload with maximum frequency of 6 rad/sec.

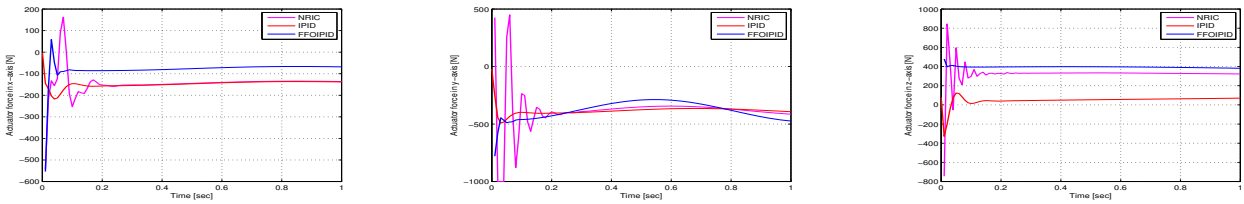

(a) Actuator force in x-axis (b) Actuator force in y-axis (c) Actuator force inz-axis

Fig. 20. Actuator forces for trajectory tracking control under maximum payload with maximum frequency of 6 rad/sec.

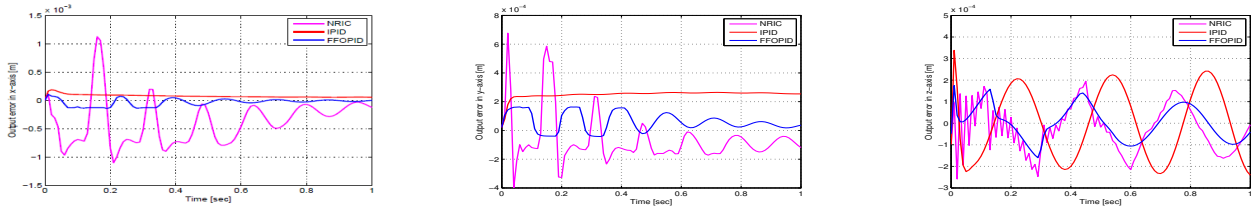

(a) Error in x-direction (b) Error in y-direction (c) Error in z-direction

Fig. 21. Joint space errors for NRIC, IPID and FFOPID during trajectory tracking control with no payload and maximum frequency of 20 rad/sec.

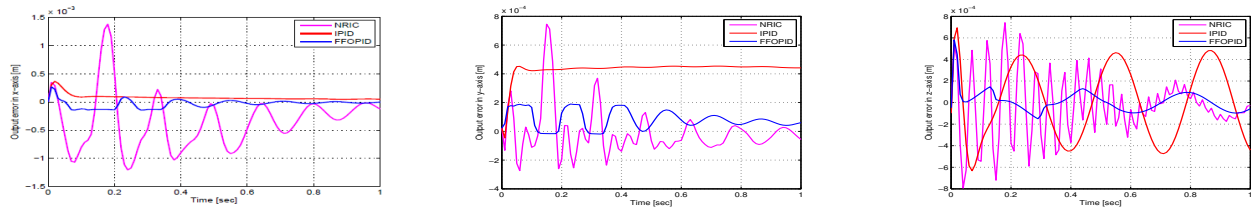

(a) Error in x-direction (b) Error in y-direction (c) Error in z-direction

Fig. 22. Joint space errors for NRIC, IPID and FFOPID during trajectory tracking control with maximum payload and maximum frequency of 20 rad/sec.

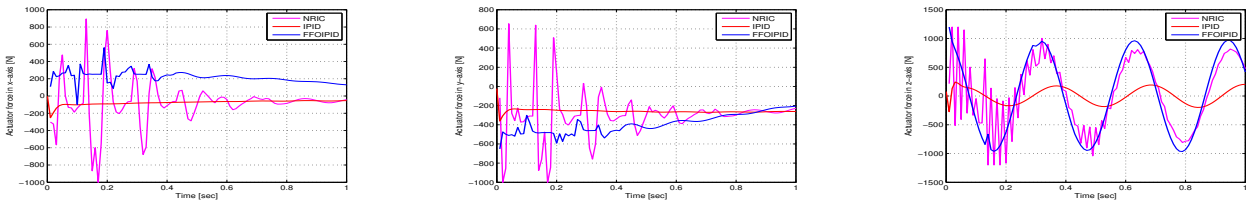

(a) Actuator force in x-axis (b) Actuator force in y-axis (c) Actuator force in z-axis

Fig. 23. Actuator forces for trajectory tracking control under no payload with maximum frequency of 20 rad/sec.

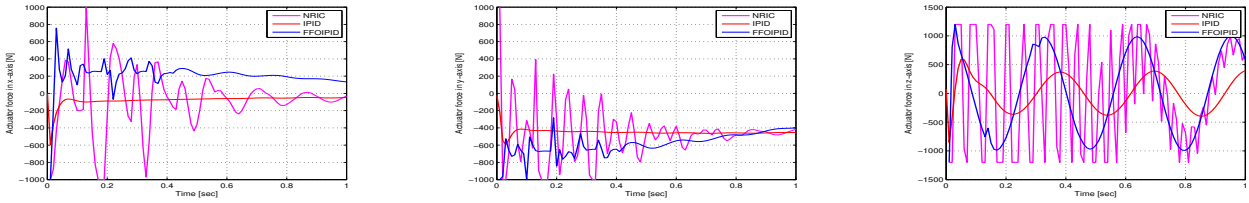

(a) Actuator force in x-axis (b) Actuator force in y-axis (c) Actuator force in z-axis

Fig. 24. Actuator forces for trajectory tracking control under maximum payload with maximum frequency of 20 rad/sec.

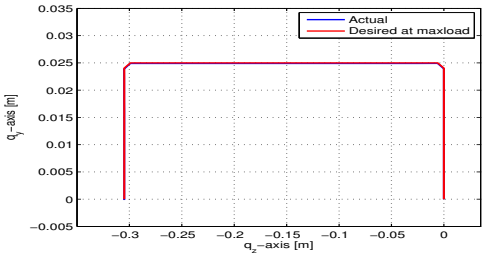

Fig. 25. Pick-and-place operation of the end-effector at yz-plane.

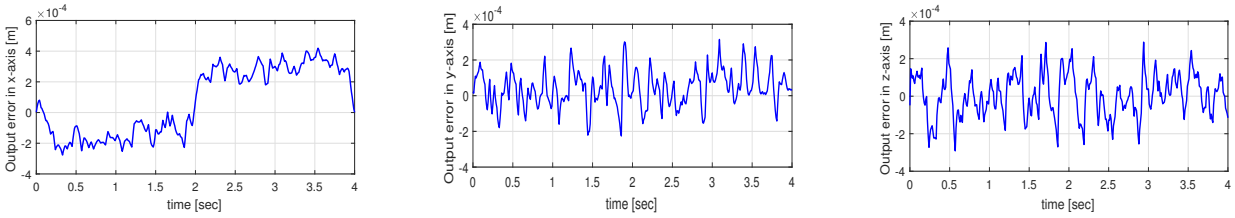

(a) Error in x-direction (b) Error in y-direction (c) Error in z-direction

Fig. 26. Joint space errors for FFOPID during trajectory tracking control with maximum frequency of 20 rad/sec and Gaussian noise of variance 10^{-9}.

$$\Omega_1 = \dot{R}_{1,\theta_1} R_1^{-1} = \begin{pmatrix} 0 & -\omega_{z1} & \omega_{y1} \\ \omega_{z1} & 0 & -\omega_{x1} \\ -\omega_{y1} & \omega_{x1} & 0 \end{pmatrix}, \quad \text{(A.4)}$$

$$\Omega_2 = \dot{R}_{2,\theta_2} R_2^{-1} = \begin{pmatrix} 0 & -\omega_{z2} & \omega_{y2} \\ \omega_{z2} & 0 & -\omega_{x2} \\ -\omega_{y2} & \omega_{x2} & 0 \end{pmatrix}, \quad \text{(A.5)}$$

then

$$\omega_1 = [\omega_{x1}\ \omega_{y1}\ \omega_{z1}], \quad \text{(A.6)}$$

$$\omega_2 = [\omega_{x2}\ \omega_{y2}\ \omega_{z2}]. \quad \text{(A.7)}$$

The potential energy of the i link is given by:

$$u_i = m_i g h_i, \quad \text{(A.8)}$$

where h_i is the vertical height from link's center of mass. The gravitational vector is considered to be with the negative y-axis $g = [0, -9.81, 0]^T$.
Abbreviations in (28-30):

$$a_1 = (b_4/b_6),\ a_2 = b_6^2,\ a_3 = (\frac{x_a^2 + z_2}{x_a^2})^{0.5}, \quad \text{(A.9a)}$$

$$a_4 = \cos(2\text{atan}\, a_1),\ a_5 = \sin(2\text{atan}\, a_1), \quad \text{(A.9b)}$$

$$a_6 = \sqrt{-\left(x_a^2+y_a^2+z_a^2\right)\left(x_a^2+y_a^2+z_a^2-\frac{1}{25}\right)}, \quad \text{(A.9c)}$$

$$a_7 = \frac{b_5}{a_6 b_6},\ a_8 = \frac{c_8}{b_6} - c_9,\ a_9 = 0.575\cos\left(\frac{c_5}{b_2}\right), \quad \text{(A.9d)}$$

$$b_1 = \sqrt{x_a^2+z_a^2},\ b_2 = \left(x_a^2+z_a^2\right)^{\frac{3}{2}}, \quad \text{(A.10a)}$$

$$b_3 = \frac{\mathrm{b_4}^2}{\mathrm{a_2}} + 1,\ b_4 = (0.2y - b_9), \quad \text{(A.10b)}$$

$$b_5 = \frac{x_a\left(4x_a^2+4y_a^2+4z_a^2-\frac{2}{25}\right)}{2}, \quad \text{(A.10c)}$$

$$b_6 = x_a^2 + \frac{\mathrm{a_3}\,x_a}{5} + y_a^2 + z_a^2, \quad \text{(A.10d)}$$

$$b_7 = \frac{b_4 {b_6}^2\left(2a_3x_a+\frac{1}{5}\right)}{a_3}, \quad \text{(A.10e)}$$

$$b_8 = 2y_a\left(x_a^2+y_a^2+z_a^2-\frac{1}{25}\right), \quad \text{(A.10f)}$$

$$b_9 = \sqrt{-\left(x_a^2+y_a^2+z_a^2\right)\left(x_a^2+y_a^2+z_a^2-\frac{1}{25}\right)}, \quad \text{(A.10g)}$$

$$c_1 = 0.575a_4,\ c_2 = b_1b_3,\ c_3 = a_5b_7, \quad \text{(A.11a)}$$

$$c_4 = \mathrm{b_8} + 2y_a, \left(x_a^2+y_a^2+z_a^2\right), \quad \text{(A.12a)}$$

$$c_5 = 2atan\left(\frac{\mathrm{b_4}}{\mathrm{b_6}}\right),\ c_6 = b_1c_7, \quad \text{(A.12b)}$$

$$c_7 = \frac{\mathrm{b_4}^2}{\mathrm{b_6}^2} + 1,\ c_8 = \frac{\mathrm{c_4}}{2\,\mathrm{b_9}} + \frac{1}{5},\ c_9 = \frac{2\mathrm{b_4}\,y_a}{\mathrm{b_6}^2}, \quad \text{(A.12c)}$$

$$e_1 = 0.5(2z_a(x_a^2+y_a^2+z_a^2-0.04)+2z_a(x_a^2+y_a^2+z_a^2)), \quad \text{(A.12d)}$$

$$e_2 = \mathrm{b_4}\left(2z_a + \frac{z_a}{5\mathrm{a_3}\,x_a}\right),\ e_3 = \frac{\mathrm{e_2}}{\mathrm{b_6}^2} - \frac{\mathrm{e_1}}{\mathrm{b_6 b_9}}. \quad \text{(A.12e)}$$

REFERENCES

[1] A. Noshadi, M. Mailah, and A. Zolfagharian, "Intelligent active force control of a 3-rrr parallel manipulator incorporating fuzzy resolved acceleration control," *Applied Mathematical Modelling*, vol. 36, no. 6, pp. 2370-2383, 2012. [click]

[2] L. Rey and R. Clavel, The delta parallel robot, In *Parallel Kinematic Machines*, Springer, pp. 401-417, 1999. [click]

[3] S. Joshi and L.-W. Tsai, "A comparison study of two 3-dof parallel manipulators: One with three and the other with four supporting legs," *IEEE Transactions on Robotics and Automation*, vol. 19, no. 2, pp. 200-209, 2003. [click]

[4] D. Kanaan, P. Wenger, and D. Chablat, "Kinematic analysis of a serial-parallel machine tool: the verne machine," *Mechanism and Machine Theory*, vol. 44, no. 2, pp. 487-498, 2009. [click]

[5] C. Gosselin and X. Kong, Cartesian parallel manipulators, US Patent 6,729,202, May 4 2004.

[6] M. Carricato and V. Parenti-Castelli, "Singularity-free fully-isotropic translational parallel manipulators," *ASME 2002 International Design Engineering Technical Conferences and Computers and Information in Engineering Conference*, American Society of Mechanical Engineer-spp. 1041-1050, 2002.

[7] X. Kong and C. M. Gosselin, "Type synthesis of linear translational parallel manipulators," *Advances in robot kinematics*, Springer, pp. 453-462, 2002.

[8] X. Kong and C. M. Gosselin, "A class of 3-dof translational parallel manipulators with linear input-output equations," *Proceedings of the Workshop on Fundamental Issues and Future Research Directions for Parallel Mechanisms and Manipulators*, pp. 25-32, 2002.

[9] C.-C. Lee and J. M. Hervé, "Cartesian parallel manipulators with pseudoplanar limbs," *Journal of Mechanical Design*, vol. 129, no. 12, pp. 1256-1264, 2007. [click]

[10] H. S. Kim and L.-W. Tsai, "Evaluation of a cartesian parallel manipulator," *Advances in robot kinematics*, Springer, pp. 21-28, 2002. [click]

[11] M. Carricato and V. Parenti-Castelli, "A novel fully decoupled two-degrees-of-freedom parallel wrist," *The International Journal of Robotics Research*, vol. 23, no. 6, pp. 661-667, 2004.

[12] M. Ruggiu, "Kinematics analysis of the cur translational manipulator," *Mechanism and Machine Theory*, vol. 43, no. 9, pp. 1087-1098, 2008.

[13] W. Li, J. Zhang, and F. Gao, "P-cube, a decoupled parallel robot only with prismatic pairs," *Mechatronic and Embedded Systems and Applications, Proceedings of the 2nd IEEE/ASME International Conference on*, IEEE, pp. 1-4, 2006.

[14] S. Briot and I. Bonev, "Pantopteron: a new fully decoupled 3dof translational parallel robot for pick-and-place applications," *Journal of Mechanisms and Robotics*, vol. 1, no. 2, p. 021001, 2009. [click]

[15] M. Magdy, M. Fanni, A. M. Mohamed, and T. Miyashita, "Kinematic design and novel mobility analysis of a new 3d pantograph decoupled manipulator," *Mechanism and Machine Theory*, vol. 117, pp. 253-275, 2017. [click]

[16] M. Lashin, M. Fanni, M. Magdy, and A. M. Mohamed, "Pd type of fuzzy controller for a new 3dof fully decoupled translational manipulator," *2016 2nd International Conference on Control, Automation and Robotics (ICCAR)*, IEEE, pp. 263-267, 2016.

[17] J. Park, W. Chung, and Y. Youm, "Analytic nonlinear h infinity optimal control for robotic manipulators," *Robotics and Automation, 1998. Proceedings. 1998 IEEE International Conference on*, vol. 3, IEEE, pp. 2709-2715, 1998.

[18] Y. Choi, W. K. Chung, and I. H. Suh, "Performance and h infinity optimality of pid trajectory tracking controller for lagrangian systems," *IEEE Transactions on Robotics and Automation*, vol. 17, no. 6, pp. 857-869, 2001. [click]

[19] M. J. Kim, S. Park, and W. K. Chung, "Nonlinear robust internal loop compensator for robust control of robotic manipulators," *International Conference on Intelligent Robots and Systems (IROS), 2012 IEEE/RSJ*, IEEE, pp. 2742-2748, 2012. [click]

[20] Y. Choi and W. K. Chung, *PID trajectory tracking control for mechanical systems*, vol. 298, Springer, 2004.

[21] D. G. Chetwynd and C. M. Gosselin, Conceptual design and dimensional synthesis of a novel 2-dof translational parallel robot for pick-and-place operations, 2004.

[22] S. Macfarlane, E. Croft, et al. "Jerk-bounded manipulator trajectory planning: design for real-time applications," *IEEE Transactions on Robotics and Automation*, vol. 19, no. 1, pp. 42-52, 2003. [click]

[23] Y. Wei, J. Qiu, and H. R. Karimi, "Reliable output feedback control of discrete-time fuzzy affine systems with actuator faults," *IEEE Transactions on Circuits and Systems I: Regular Papers*, 2016.

[24] Y. Wei, J. Qiu, H. R. Karimi, and M. Wang, "Model reduction for continuous-time markovian jump systems with incomplete statistics of mode information," *International Journal of Systems Science*, vol. 45, no. 7, pp. 1496-1507, 2014. [click]

[25] Y. Wei, J. Qiu, H. R. Karimi, and M. Wang, "Model approximation for two-dimensional markovian jump systems with state-delays and imperfect mode information," *Multidimensional Systems and Signal Processing*, vol. 26, no. 3, pp. 575-597, 2015. [click]

[26] Y. Wei, J. Qiu, and H. R. Karimi, "Quantized $\mathcal{H}_\infty$ filtering for continuous-time markovian jump systems with deficient mode information," *Asian Journal of Control*, vol. 17, no. 5, pp. 1914-1923, 2015. [click]

[27] Y. Wei, J. Qiu, H. R. Karimi, and M. Wang, "Filtering design for two-dimensional markovian jump systems with state-delays and deficient mode information," *Information Sciences*, vol. 269, pp. 316-331, 2014. [click]

Manar Lashin was born in Kalyobiya, Egypt, in 1987. She has received the B.Sc. in control and measurements from Benha University, Kalyobiya, Egypt and received the M.Sc. degree in mechatronics and robotics from Egypt-Japan University of Science and Technology (EJUST), Alexandria, Egypt. She is currently working toward a Ph.D. degree in mechatronics and robotics at EJUST. Her research interests include nonlinear control, robust control, robot kinematics, dynamic and modeling.

Mohamed Fanni received the B.E. and M.Sc. degrees in mechanical engineering from Faculty of Engineering of both Cairo University and Mansoura University, Egypt, in 1981 and 1986, respectively and the Ph.D. degree in engineering from Karlsruhe University, Germany, 1993. He is a Professor with the Dept. of Mechatronics and Robotics Engineering Egypt-Japan University of Science and Technology E-JUST, Alexandria, on leave from Production Engineering and Mechanical Design Department, Faculty of Engineering, Mansoura University, Egypt. His major research interests include robotics engineering, automatic control, and Mechanical Design. His current research focuses on Design and Control of Mechatronic Systems, Surgical Manipulators, Teleoperation systems and Flying/Walking Robots.

Abdelfatah Mohamed received the Ph.D. degree from University of Maryland, College Park, USA in 1990. Since 1990 he has been an Assistant Professor with the Dept. of Electrical Engineering, Assiut University, Egypt. He became an Associate Professor in 1995, and Professor in 2000. From September 1990 to August 1993, He has been a Postdoctoral Fellow at the Dept. of Mechanical Engineering, University of Texas, Austin USA. From April 1996 to April 1997, He has been a visiting Professor at the Dept. of Electrical Engineering, Kanazawa University, Japan. From September 2010 to March 2012 He has been the Head, Dept. of Electrical Engineering, Assiut University, and became the Dean of Faculty of Engineering, Assiut University on March 2012. Currently, he is the Head of the Dept. of Mechatronics and Robotics Engineering, Egypt-Japan University of Science and Technology. His research interest lies in Robust and Intelligent control, Magnetic Bearing systems, Robotics, Industrial drives. Dr. Mohamed is a senior IEEE member.

Tomoyuki Miyashita was born in Japan in 1968. He received the B.E., M.E., and Ph.D. degrees from Waseda University, Tokyo, Japan, in 1990, 1992, and 2001, respectively. He joined Nippon Steel Corporation, Tokyo, Japan, in 1992. Since 1998, he has been with the Graduate School of Engineering, Waseda University, where he is currently a Professor. His main areas of research interest are mechanical design considering dynamical properties, flexible space structures, and their control systems. Dr. Miyashita is a member of The Japan Society of Computer Aided Surgery, The Japan Society of Mechanical Engineers, Japan Society for Design Engineering, The American Institute of Aeronautics and Astronautics, The Institute of Electrical and Electronics Engineers.